

Formation of the muonic helium atom

P. A. Souder, T. W. Crane,* V. W. Hughes, D. C. Lu, H. Orth,[†] H. W. Reist,[‡] and M. H. Yam
Yale University, Gibbs Laboratory, Physics Department, New Haven, Connecticut 06520

G. zu Putlitz

University of Heidelberg, D69, Heidelberg, Germany

(Received 28 September 1979)

A full description is given of an experiment in which the muonic helium atom, ${}^4\text{He}\mu^-e^-$, was first observed. The method of the experiment was to study the precession of the magnetic moment of negative muons stopped in 14-atm helium with a 2% Xe admixture. A signal at the characteristic Larmor frequency of the atom was observed with an amplitude which corresponds to a muon residual polarization of $5.0 \pm 0.7\%$. In pure helium at 14 atm, precession characteristic of free muons with a polarization of $5.8 \pm 1.3\%$ was found. The hyperfine structure of ${}^4\text{He}\mu^-e^-$ and the various processes involved in the formation of this atom are also discussed.

I. INTRODUCTION

The muonic helium atom, ${}^4\text{He}\mu^-e^-$,¹ is the neutral atomic system composed of a helium nucleus, a negative muon, and an electron. With most muonic atoms interest lies in the interaction of the muon with the nucleus, and the presence of any orbital electrons is treated as an unwanted perturbation. In the case of the muonic helium atom, however, we are primarily interested in the muon-electron interaction. The present method of studying this atom² is to observe the precession of the muon spin, which is coupled to the spin of the electron by the hyperfine interaction. This coupling results in a different precession frequency than would occur were the muon free or part of a muonic helium ion $({}^4\text{He}\mu^-)^+$. By this precession method, $P_{1/2}$ and $P_{3/2}$ electronic states of $\mu^- \text{Ne}$ have previously been identified.^{3,4}

The muonic helium atom⁵ is of special interest because it is the simplest atom of this general type.⁶ The calculation of the wave functions is a tractable problem which can be solved to much higher precision than possible for an atom with many electrons. In analogy to the case for muonium, the ability to prepare polarized muonic helium atoms makes possible precision measurements of its hyperfine structure interval $\Delta\nu$ and of its Zeeman effect. Such spectroscopic data can be used to test the atomic structure calculations or alternatively to provide information about the fundamental muon-electron interaction and the muon magnetic moment.

II. THEORY OF THE ATOM

The atom ${}^4\text{He}\mu^-e^-$ is the simplest muon-electron atom with an atomic nucleus. From one point of view it is analogous to helium in which one elec-

tron is replaced by a negative muon. Indeed the proper starting point for the theory of this atom is the analog of the Breit equation for helium. From another viewpoint, it is similar to hydrogen in which the proton is replaced by the pseudonucleus $({}^4\text{He}\mu^-)^+$, since the radius of the muonic orbit in the 1S state of the muonic helium atom is small compared to that of the electron. The electron sees a pseudonucleus with a unit positive charge and a magnetic moment equal to that of a negative muon. Hence the hyperfine structure (hfs) interval $\Delta\nu$ in the ground state will be approximately equal to that of muonium (μ^+e^-), but inverted because of the different signs of the magnetic moments of μ^+ and μ^- . Apart from the reduced mass correction, the principal difference between $\Delta\nu$ for muonium and $\Delta\nu$ for ${}^4\text{He}\mu^-$ is due to the finite size of the pseudonucleus $({}^4\text{He}\mu^-)^+$ and the penetration of the electron inside this structure.⁷ This effect gives a term of relative order m_e/m_μ , and is similar to the hfs anomaly^{8,9} first observed for deuterium and due to the penetration of the electron inside the deuteron.

The theoretical value of $\Delta\nu$ for ${}^4\text{He}\mu^-e^-$ can be written^{10,11}

$$\Delta\nu = \Delta\nu_F (1 + \delta^{\text{rel}} + \delta^{\text{rad}} + \delta^{\text{rec}}) \quad (2.1)$$

or

$$\Delta\nu = \Delta\nu_F [1 + C_1\alpha + C_2\alpha^2 + C_3\alpha(m_e/m_\mu) \ln(m_\mu/m_e)]$$

where $\Delta\nu_F$ is the leading Fermi term, and δ^{rel} , δ^{rad} , and δ^{rec} refer to relativistic, radiative, and recoil contributions. Evaluation of $\Delta\nu_F$ has recently been done by a variational calculation¹¹ and also by a second-order perturbation approach.¹² The relativistic, radiative, and recoil contributions determine^{11,13} $C_1 = 1/\pi$, $C_2 = -1.57$, and $C_3 = -0.073$. Values given for $\Delta\nu_F$ by Huang and Hughes¹¹ and by Lakdawala and Mohr¹² are (4465.1 ± 1.0) and $(4462.6$

± 3.0 MHz, respectively, in which the estimated errors arise from the calculation of $\Delta\nu_F$.

In a static external magnetic field, the relevant part of the Hamiltonian for the ground state of ${}^4\text{He}\mu^-e^-$ is given by

$$\mathcal{H} = a\vec{I}_\mu \cdot \vec{J} + \mu_B^e g_J \vec{J} \cdot \vec{H} + \mu_B^\mu g'_\mu \vec{I}_\mu \cdot \vec{H}, \quad (2.2)$$

where $a = -h\Delta\nu$ is the hfs coupling constant, \vec{I}_μ is the muon spin operator, \vec{J} is the electronic angular-momentum operator, g_J (g'_μ) is the electron (muon) gyromagnetic ratio in ${}^4\text{He}\mu^-e^-$, and \vec{H} is the static external magnetic field. The quantities g_J and g'_μ are approximately related to the free-particle values g_e and g_μ by^{14,15}

$$g_J \cong g_e \left(1 - \frac{1}{3}\alpha^2\right) = 2(1.00114), \quad (2.3)$$

$$g'_\mu \cong g_\mu \left(1 - \frac{4}{3}\alpha^2\right) = 2(1.00109), \quad (2.4)$$

where small screening corrections are neglected and where the experimental values for g_e (Ref. 16) and g_μ (Ref. 17) are

$$g_e = 2(1.0011596524) \pm 0.2 \text{ and}$$

$$g_\mu = 2(1.001165937) \pm 12 \text{ ppb.}$$

The eigenvalues of this Hamiltonian are given by the Breit-Rabi formula,^{18,19}

$$W_{F(\pm\frac{1}{2}\pm\frac{1}{2}), M_F} = \frac{1}{2}h\Delta\nu + \mu_B^\mu g'_\mu M_F H \mp \frac{1}{2}h\Delta\nu(1 - 2M_F x + x^2)^{1/2}, \quad (2.5)$$

where F is the total-angular-momentum quantum number, M_F is the associated magnetic quantum number, and $x = (\mu_B^e g_J - \mu_B^\mu g'_\mu)H/h\Delta\nu$. Numerically $x = H/1601$ G. Figure 1 shows the energy-level diagram. Note the inversion relative to muonium due to the fact that a is negative. The transition frequencies of greatest interest for magnetic resonance studies are ν_{12} , ν_{14} , ν_{13} , and ν_{34} . They are given below, and ν_{12} and ν_{34} are plotted in Fig. 2.

$$\nu_{12} = \frac{W_{0,0} - W_{1,1}}{h} = -\frac{\mu_B^\mu g'_\mu H}{h} + \frac{1}{2}\Delta\nu[1 - x + (1+x^2)^{1/2}],$$

$$\nu_{34} = \frac{W_{1,0} - W_{1,-1}}{h} = \frac{\mu_B^\mu g'_\mu H}{h} + \frac{1}{2}\Delta\nu[1 + x - (1+x^2)^{1/2}],$$

$$\nu_{14} = \frac{W_{0,0} - W_{1,-1}}{h} = \frac{\mu_B^\mu g'_\mu H}{h} + \frac{1}{2}\Delta\nu[1 + x + (1+x^2)^{1/2}],$$

$$\nu_{13} = \frac{W_{0,0} - W_{1,0}}{h} = \Delta\nu[(1+x^2)^{1/2}]. \quad (2.6)$$

The magnetic moments of the four states are given by

$$\mu_{F, M_F} = -\frac{\partial W_{F, M_F}}{\partial H}, \quad (2.7)$$

$$\mu_{\pm\frac{1}{2}, 0} = \frac{\pm\frac{1}{2}x}{(1+x^2)^{1/2}}(\mu_B^e g_J - \mu_B^\mu g'_\mu), \quad (2.8)$$

$$\mu_{1, \pm 1} = \mp\frac{1}{2}(\mu_B^e g_J + \mu_B^\mu g'_\mu).$$

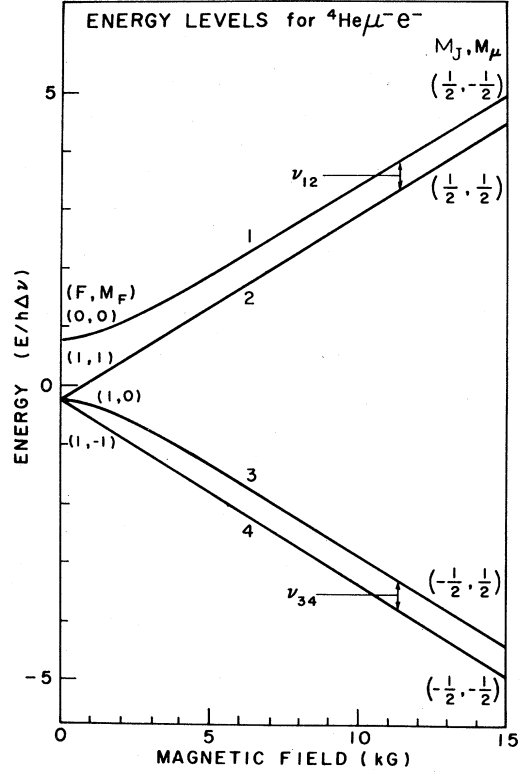


FIG. 1. Energy-level diagram for ${}^4\text{He}\mu^-e^-$ in the ground state in a magnetic field, as given by Eq. (2.5). The states are labeled 1-4 for convenience.

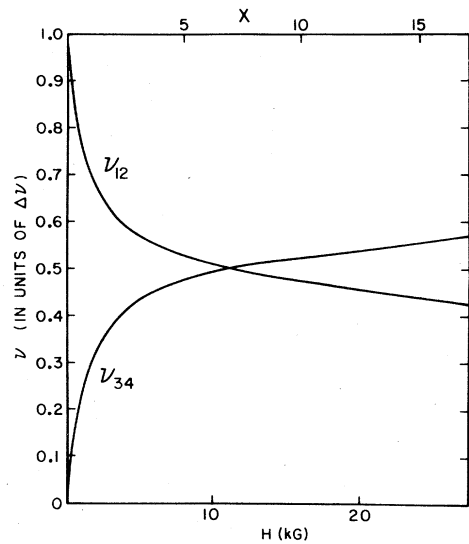


FIG. 2. Plot of resonance frequencies ν_{12} and ν_{34} vs x or H , as given by Eq. (2.6).

Finally, the spin eigenfunctions $\chi_{F, M_F}(H)$ can be expressed in terms of the strong-field spin eigenfunctions α_μ , β_μ , and $\alpha_e\beta_e$:

$$\begin{aligned}\chi_{0,0}(H) &= c\beta_e\alpha_\mu - s\alpha_e\beta_\mu, \\ \chi_{1,1}(H) &= \alpha_e\alpha_\mu, \\ \chi_{1,0}(H) &= c\alpha_e\beta_\mu - s\beta_e\alpha_\mu, \\ \chi_{1,-1}(H) &= \beta_e\beta_\mu,\end{aligned}\quad (2.9)$$

where $\alpha_\mu(\beta_\mu)$ is the normalized spin eigenfunction for μ^- ; $\alpha_\mu(\beta_\mu)$ corresponds to spin orientation in the positive (negative) z direction. Also $\alpha_e(\beta_e)$ is the similarly defined electron-spin eigenfunction. The quantities $s(H)$ and $c(H)$ are given by

$$\begin{aligned}s &= 2^{-1/2}[1 + x/(1+x^2)^{1/2}]^{1/2}, \\ c &= 2^{-1/2}[1 - x/(1+x^2)^{1/2}]^{1/2}.\end{aligned}\quad (2.10)$$

Equations (2.2)–(2.9) are very similar to the corresponding equations for muonium.²⁰ The only differences in addition to the slight difference in $\Delta\nu$ are the opposite signs of g'_μ and the hfs coupling constant a . However, these sign differences result in significant variations in the energy-level diagrams (see Figs. 1 and 2).

The method of our experiment is the classic and usual one for studying the Larmor precession of muonium or of free muons.²⁰⁻²² A beam of polarized muons is stopped in a suitable gas target placed in a uniform static magnetic field. The muon moments precess due to the magnetic field at a Larmor frequency f_L characteristic of their final chemical environment. In $({}^4\text{He}\mu^-)^+$, the muon moment precesses at approximately the Larmor precession frequency of a free muon. The gyromagnetic ratio is then given by (in kHz/G)

$$\gamma \equiv \frac{f_L \mu}{H} = \frac{\mu_\mu}{\hbar I} = 13.554, \quad (2.11)$$

where $\mu_\mu = g'\mu_B^\mu$ and $I = \frac{1}{2}$ is the angular momentum of the muon.

The muonic helium atom in its ground state has four levels as given in Eq. (2.9). If $M_F = \pm 1$ then, in the limit of a weak magnetic field H in the x direction, the atomic magnetic moment μ_{F, M_F} will precess with a gyromagnetic ratio of (in MHz/G)

$$\gamma({}^4\text{He}\mu^-e^-) = \frac{\mu_{1,1}}{\hbar H} = \frac{g'_\mu \mu_B^\mu + g'_e \mu_B^\mu}{2\hbar} = 1.408. \quad (2.12)$$

This is very near the value of the gyromagnetic ratio for muonium in the $(F, M_F) = (1, 1)$ level of

$$\gamma_M = 1.394 \quad (2.13)$$

in MHz/G. For states with $M_F = 0$, $\mu = \gamma = 0$, and

there is no precession of the atom. Typically half of the ${}^4\text{He}\mu^-e^-$ are produced with $M_F = \pm 1$ and half with $M_F = 0$.

III. RESIDUAL POLARIZATION AND FORMATION OF ${}^4\text{He}\mu^-e^-$

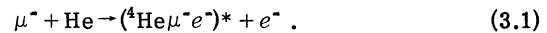
A necessary condition for observing ${}^4\text{He}\mu^-e^-$ in our experiment is that polarized muons stopping in helium gas retain some polarization and finally form the polarized muonic helium atom. In this section we discuss the numerous processes that determine what the residual polarization of the muon and formation fraction of the atom will be.

A. Residual polarization of negative muons stopped in helium

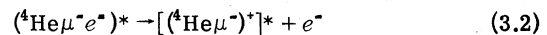
The study of negative muons stopping in various media has revealed many interesting phenomena. Extensive experimental and theoretical work has been done on this subject, and a number of reviews have been published.²³⁻²⁵ Owing to the complexities of the processes involved, our understanding of the subject is still rather incomplete, even for the relatively simple case where the stopping medium is helium gas.

Slow negative muons traversing a medium lose most of their energy through ionization and atomic excitation, get captured by an atom into a highly excited state, cascade down to the ground state, and interact with the surrounding medium before decaying or undergoing nuclear capture. For our experiment it is essential to have a nonzero residual polarization at the end of this chain, and we emphasize the effects of each of these processes on the muon polarization.

Initially the muons are polarized parallel to the beam direction. Before capture the direction of the momentum of a given muon is randomized by collisions, but the polarization relative to the laboratory is preserved.²⁶ When the muon velocity becomes sufficiently low, $\approx \alpha c$, capture by an atom occurs by means of an Auger process:



Here the asterisk denotes an excited state, probably with the muon principal quantum number n near 14.²⁷ For high- n orbits, the Auger transition



has a much higher probability than radiative transitions, and the atom is ionized. Auger transitions favor $\Delta n = 1$, so the muon is still highly excited. The muon now cascades down to the ground state. Radiative transitions, which are relatively slow for large- n orbits of low- Z atoms, are the only available channel for the cascade in the ab-

sence of other atoms supplying further electrons for Auger processes. Due to the spin-orbit coupling, the muon is partially depolarized when in these excited states. Calculations of the residual polarization at the end of the cascade, including the effects of Auger capture, Auger transitions, and radiative transitions, yield values of 15–20%.^{26,28}

Agreement with this simple theory has been reported for several materials, including C, Mg, Si, Cd, and Pb.^{29,30} In many other materials, additional depolarizing mechanisms are present, often involving interactions with electrons in paramagnetic states.²³ In helium, both in liquid and gaseous phases, experiments have found anomalously low values for the residual polarization.^{2,31–33} One conceivable explanation for the low polarization might be the formation of the paramagnetic atom ${}^4\text{He}\mu^-e^-$. However, Larmor precession characteristic of this atom was not found in liquid helium.³² And indeed formation of ${}^4\text{He}\mu^-e^-$ in He gas is not to be expected because in the early part of the cascade all electrons are ejected in Auger processes leaving $({}^4\text{He}\mu^-)^+$ and, because of the 11-eV difference in ionization potentials between ${}^4\text{He}\mu^-e^-$ and ordinary helium, it is not energetically possible for $({}^4\text{He}\mu^-)^+$ to capture an electron from a He atom. The additional depolarization is probably due to depolarizing collisions during the cascade, as will be discussed in more detail below.

The specific place of helium in the periodic table has important consequences for the cascade. In contrast to muonic hydrogen, which is a neutral object that penetrates inside neighboring atoms where deexcitation can occur due to Stark mixing, muonic helium rapidly becomes an ion. Atoms of next-higher Z , Li, and Be, commonly occur in solids where Auger electrons can be quickly replaced, and the cascade is characterized by many Auger transitions. For atoms of still-higher Z , many electrons are naturally available for Auger transitions and also radiative transitions are faster. Hence $({}^4\text{He}\mu^-)^+$ has the unique feature of being formed in an excited state which lives long enough so that collisions with neighboring helium atoms may play an important role in the cascade.

Theoretical calculations of the cascade time for helium³⁴ find that both external Auger electrons and collisional Stark mixing greatly reduce the cascade time expected for the free atom. These calculations predict times about 100 times faster than the observed value³⁵ which itself is faster than the value expected without collisions. Measurements of cascade x rays and the 2S metastable yield made in helium gas^{36,37} have also demonstrated the importance of collisional Stark mixing

and external Auger transitions; in particular, the 2S yield is a factor of 2 higher than possible in vacuum. Comparisons of gaseous to liquid helium have shown that cascade times are similar³⁵ but that x-ray yields are very different.³⁶

To our knowledge, no theoretical studies have been made of the effect of collisions on the residual polarization of $({}^4\text{He}\mu^-)^+$. Since many of these collisions occur when the $({}^4\text{He}\mu^-)^+$ ion is in high n orbits which have radial dimensions comparable to those of atoms, it is justified to draw some conclusions from analogies between the depolarization of atomic atoms and ions with nonzero orbital angular momentum and excited muonic helium ions. Cross sections for the depolarization of atomic P states range between 50 \AA^2 ($\text{Na } {}^3P_{1/2}\text{-He}$) and 300 \AA^2 ($\text{Cs } {}^2P_{3/2}\text{-Xe}$).³⁸ Depolarization in these collisions is due to the nonresonant electrostatic-induced dipole-dipole interaction.^{39,40} Recent theoretical calculations agree with these experimental data within a factor of 2.⁴¹ Neglecting numerical factors, the cross section is proportional to

$$\sigma \sim \langle r^2 \rangle \alpha / \bar{v}_{rel}^2, \quad (3.3)$$

where $\langle r^2 \rangle$ is the expectation value for the square of the radial coordinate for μ^- in $({}^4\text{He}\mu^-)^+$, α is the polarizability of the buffer gas, and \bar{v}_{rel} is the average relative velocity of the collisions.⁴¹ Since these parameters are similar for the case of excited $({}^4\text{He}\mu^-)^+$, we would expect similar cross sections. From measurements of excited ionic states⁴² it is known that the additional ionic charge tends to enhance the depolarization slightly but no more than by a factor of 2. The conclusion has to be drawn that collisional depolarization may well be responsible for the observed loss of polarization in the formation of $({}^4\text{He}\mu^-)^+$ unaccounted for by other processes.

Depolarization associated with formation of the molecular ion $({}^4\text{He}\mu^-)^+\text{He}$ and caused by its rotational magnetic fields is another conceivable process but probably less likely than the collision depolarization just discussed.^{43–45}

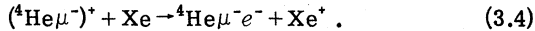
As explained in the next section, we also used an admixture of He plus 2% Xe in order to form the atom ${}^4\text{He}\mu^-e^-$ in the ground state. We note here that since this amount of Xe provides a significant fraction of the electrons in the gas, its presence could also influence the cascade. In particular, if the Xe increases the deexcitation rate of the $[({}^4\text{He}\mu^-)^+]$ through the external Auger effect, the resulting decrease in the lifetimes of the highly excited states could result in a larger residual polarization than in pure He.

For our experiment it is important to know that

the $({}^4\text{He}\mu)^+$ ions are at least partially polarized. Since the present theory gives no quantitative estimate of what the total depolarization should be, an important part of the experiment is to measure the polarization of the $({}^4\text{He}\mu)^+$ ions formed when muons are stopped in pure helium.

B. Formation of the ${}^4\text{He}\mu^-e^-$ atom

To form the ${}^4\text{He}\mu^-e^-$ atom from the $({}^4\text{He}\mu^-)^+$ ion, we must provide an electron donor with an ionization potential less than 13.6 eV. We chose Xe (Refs. 7 and 46) so that the reaction is



The quantity of Xe that must be added depends on the cross section for this reaction and also upon the existence of any competing reaction.

No direct information on the reaction of Eq. (3.4) exists, but data for the similar reaction with hydrogen,



does⁴⁷ and is given in Fig. 3. Cross sections for $({}^4\text{He}\mu^-)^+$ or μ^+ should be approximately the same at the same velocity, at least for high energies. The hydrogen cross section has a broad maximum with a value of $4 \times 10^{-15} \text{ cm}^2$, but drops rapidly at lower energies corresponding to velocities below

$$v = a|\Delta E|/\hbar, \quad (3.6)$$

where a is a distance characterizing the potential and ΔE is the kinetic energy gained or lost in the reaction.⁴⁸ Only two states of Xe^+ , ${}^2P_{1/2}$ and ${}^2P_{3/2}$, are energetically possible at thermal energies in Eq. (3.4), and both have nearly the same energy. Hence no additional maxima are expected at lower energies. Since the $({}^4\text{He}\mu^-)^+$ ions are rapidly

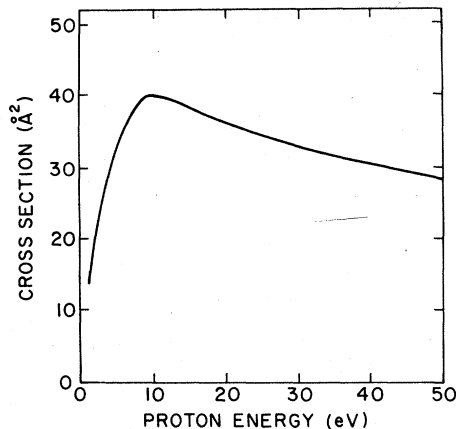
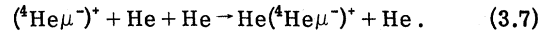


FIG. 3. Plot of the cross section for $\text{H}^+ + \text{Xe} \rightarrow \text{H} + \text{Xe}^+$, from Ref. 47.

thermalized, the relevant energy is well below that corresponding to the critical velocity of Eq. (3.6) and also below the velocities of Fig. 3. In view of the expected rapid increase with energy, cross sections as small as 10^{-16} or 10^{-17} cm^2 are possible at thermal energies. At the low energies the usual semiclassical approximations are invalid, and it is difficult to make a more precise estimate.

A possible competing reaction is molecular-ion formation⁴²:

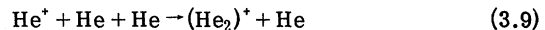


This reaction is necessarily ternary to accommodate energy-momentum conservation. The binding energy for $(\text{HeH})^+$ is 1.7 eV,⁴⁹ and that for $({}^4\text{He}\mu^-)^+$ should be approximately the same. Thus once the molecular ion is formed, reactions with Xe are energetically forbidden. Since the molecular ion is diamagnetic, its formation will have only a very small influence on the muon precession frequency.

The reaction rate for molecular-ion formation may be written in the phenomenological form⁴⁴

$$\lambda = n^2 \sigma v V, \quad (3.8)$$

where λ is the rate, n is the atomic number density, σ is an appropriate cross section, v is the ion velocity, and V is the three-body interaction volume. Estimating λ is difficult because (1) λ depends on the relevant interaction radius to the fifth power and (2) λ is quite sensitive to the details of molecular orbits. One estimate is $\lambda({}^4\text{He}\mu^-)/n^2 = 6 \times 10^{-35} \text{ cm}^6/\text{sec}$.⁴⁴ The measured rate for the somewhat similar reaction



is $\lambda({}^4\text{He}\mu^-)/n^2 = 1.08 \pm 0.005 \times 10^{-31}/\text{sec}$.⁵⁰ For our conditions (15 atm) these rates are $\lambda({}^4\text{He}\mu^-) = 1.0 \times 10^7/\text{sec}$ and $\lambda(\text{He}) = 1.6 \times 10^{10}/\text{sec}$. Since both numbers are higher than the muon decay rate, it seems likely that molecular ions are formed. Moreover, $\lambda({}^4\text{He}\mu^-)$ may be comparable to the rate for the reaction of Eq. (3.4), even with high Xe concentration.

Some information about the above reactions is provided by studies of positive muons stopped in He and He-Xe mixtures.⁵¹ When positive muons stop in pure helium, no muonium is formed and a free muon spin precession signal is observed. Adding 0.09% Xe quenches the free muon signal (13 kHz/G) and produces a muonium signal (14 MHz/G). This signal implies that the muonium is formed rapidly so that all of the spins start precessing at the same time relative to the respective muon stops. With a Xe admixture of 0.015%, a large free muon signal is observed which persists during the entire lifetime of the

muons. In view of the rapid formation of muonium with only six times more Xe, we conclude that the muonium is formed before the μ^+ are thermalized. Muonium formation fractions in He-Xe mixture can be explained in terms of known cross sections for hydrogen (Fig. 3) even if it is assumed that no reactions occur at thermal energies. The inertness of free muons at thermal energies can be due to either a small Xe cross section⁵² of less than 3×10^{-19} cm² or molecular-ion formation. Since this cross section for Xe seems unreasonably small, we favor the hypothesis that molecular ions are formed.

The μ^+ results cannot be directly applied to the $({}^4\text{He}\mu^-)^+$ case because of the large difference in mass of these two ions. A positive muon is forty times lighter than a helium atom and thus loses little energy during an elastic collision. Consequently, it spends considerable time at energies on the order of 10 eV, where the Xe cross section is large and where no other inelastic channels are open. In contrast, $({}^4\text{He}\mu^-)^+$ has nearly the same mass as a helium atom and will thermalize rapidly through elastic collisions, possibly even before the end of the cascade. Thus ${}^4\text{He}\mu^-e^-$ must be formed at nearly thermal energies, and high Xe concentrations are probably required.

The formation of the molecular ion $\text{He}({}^4\text{He}\mu^-)^+$ is also relevant to experiments studying $({}^4\text{He}\mu^-)^+$ in the metastable 2S state. In particular, if a molecular ion is formed, the quenching rate of the 2S state is calculated⁴⁴ to be much higher than the observed quenching rate.³⁷ An alternative explanation is that two or more helium atoms are bound in a symmetrical configuration which is less likely to induce quenching.³⁷ We note that the theoretical quenching rate due to collisions,^{37,45} even apart from any molecular-ion formation, is much larger than experimentally observed.

In view of the above considerations, it is not clear how much Xe must be added to the He in order to form ${}^4\text{He}\mu^-e^-$, other than that the 0.1% concentration required for muonium formation is probably a lower bound. Although molecular-ion formation is probably an important competing reaction, this has not been conclusively established. We note that for noble-gas mixtures the probability for muon capture by a given nucleus is given approximately by the Z law.^{53,54} Thus for Xe admixtures greater than several percent most of the negative muons would be captured by the Xe.

Because of the small charge-exchange cross section of Xe at low energy and also the competitive nature of the formation of ${}^4\text{He}\mu^-e^-$ and the capture of negative muons by Xe, this heavy atom may not be the ideal formation agent. Low- Z molecules like CH_4 or C_2H_6 , with their rich elec-

tronic spectra advantageous for nearly resonant charge-exchange cross sections, may be superior. These molecules also have low ionization potentials and should have small depolarizing cross sections, conditions which are indispensable for the formation of polarized neutral muonic helium atoms.

IV. EXPERIMENTAL METHOD AND APPARATUS

A. General method of the experiment

The precession of the muons in a magnetic field is observed by detecting the decay electrons, which are emitted preferentially in the direction of the muon spin according to the distribution

$$N(\theta) \approx 1 + a \cos\theta, \quad (4.1)$$

where a is the analyzing power of the decay and θ is the angle between the direction of the fixed counter telescope and the muon spin. The value of a depends on the energy of the decay electron and has an average value of $\frac{1}{2}$. For a small fixed electron telescope, this results in the following time spectrum:

$$N(t) \approx e^{-t/\tau} (1 + a \cos 2\pi\gamma H t), \quad (4.2)$$

where τ is the muon lifetime in the stopping material. For ${}^4\text{He}\mu^-e^-$, there is the loss of an extra factor of 2 in amplitude because only half the atoms, those with $M_F = \pm 1$, participate in the precession; thus $a^M = \frac{1}{2}a^\mu$ where the superscript M refers to the atom and the superscript μ refers to free muon precession. In this paper, a^M and a^μ refer to a phenomenological analyzing power defined by Eq. (4.2) and include all effects such as beam polarization, finite solid angle, etc., that determine the signal height.

A diagram of the apparatus is shown in Fig. 4. In the right-handed coordinate system shown, the initial negative muon polarization is in the positive z direction, the magnetic field is in the x direction, one telescope ($e_F = E_1E_2$) is in the z direction, and the other ($e_D = E_3E_4$) is in the negative y direction.

B. Beam and target

Muons from the cyclotron at the Space Radiation Effects Laboratory stopped in the gas target shown in Fig. 4. The beam has a polarization of 0.65 and a momentum of 100 MeV/ c . A range curve is given in Fig. 5. It has a full width at half maximum (FWHM) of 2.8 g/cm² of polyethylene. This width corresponds to about 50 times the material in the target operated at typical conditions (14 atm of helium). Thus target-empty data can be subtracted from target-full data without worry that the absence of the relatively small amount of

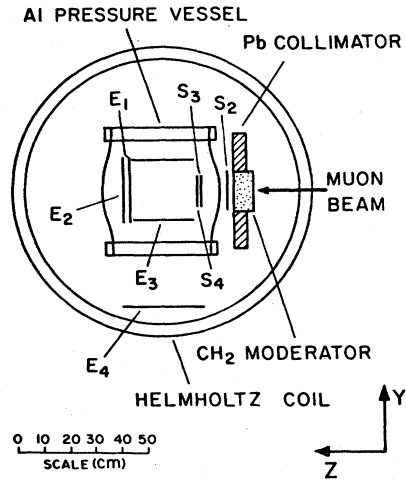


FIG. 4. Schematic diagram of apparatus to search for the precession of $({}^4\text{He}\mu^-)^+$ and ${}^4\text{He}\mu^-e^-$. S_1 is upstream and not shown. The magnetic field points out of the paper.

target gas will influence the distribution of background wall stops.

The target gas consisted of helium often mixed with a small concentration of xenon ($\leq 2\%$) in a cylindrical pressure vessel. The pressure vessel, described elsewhere,⁵⁵ was modified by adding a light-guide port for an additional scintillation counter to detect wall stops.

The helium used was produced with less than one ppm total impurities.⁵⁶ The Xe had about 25-ppm impurities, mostly Kr.⁵⁷ Care was taken to maintain the gas purity by evacuating the pressure vessel to 10^{-4} Torr before adding gas. Also, the gas was circulated over hot Ti at 750°C at a rate of 15 l/hr. Thus the entire 48-l volume of the pressure vessel was purified once every 3 h on the average. This procedure is very efficient at removing paramagnetic impurities such as O_2 which could depolarize ${}^4\text{He}\mu^-e^-$ atoms. Probably the dominant impurities remaining were hydrocarbons emitted by the plastic scintillators and

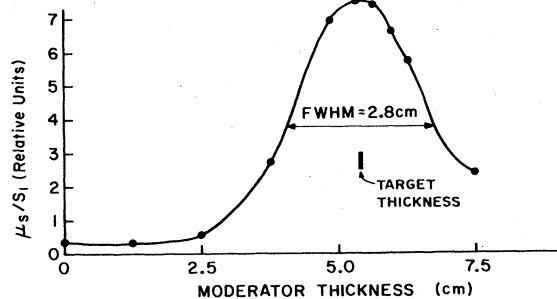


FIG. 5. Range curve for the muon beam obtained by measuring the stopping rate as a function of the amount of moderator. The thickness of the target filled with 14-atm He is also indicated on the same scale.

light guides present in the pressure vessel. However, this sort of impurity should be unimportant for these studies.

C. Magnetic field

The magnetic field for the Larmor precession was produced by four pairs of Helmholtz coils. Three mutually orthogonal pairs, 140 cm in diam, nulled out the earth's magnetic field and the fringe field of the cyclotron magnet and also produced low magnetic fields up to 4.6 G that were suitable for ${}^4\text{He}\mu^-e^-$ precession. A fourth pair of Helmholtz coils, 95 cm in diameter, produced a high field of 67 G suitable for observing free muon precession.

Adequate spatial uniformity of the magnetic field over the active volume of the target was required to keep all of the muons precessing in phase during the observation time. For Helmholtz coils, the theoretical nonuniformity is approximately bounded by $(D/D_0)^4$ where D is the diameter of the volume of interest and D_0 is the diameter of one of the coils. For a 24-cm-diam spherical target, this implies a 0.1% deviation for the low-field configuration and a 0.5% deviation for the high-field configuration. In both cases this nonuniformity should have a negligible effect on the data.

The dominant nonuniformity turned out to be a gradient in the fringe field of the cyclotron magnet. This effect was measured and found to be well described by the following function:

$$\Delta|\vec{H}| = (-6.5x + 4.6y - 9.0z) \quad (4.3)$$

in mG/cm. The coordinates are defined in Fig. 4. The field maps (~15 data points per field) agreed with this function to about ± 10 mG independent of field at low fields. This nonuniformity is negligible for the data obtained with a 67-G field, but was important for the analysis of data taken at < 5 G.

The current through the coils was measured with precision shunts and a digital volt meter. Short-term regulation was good, and long-term drifts were observed to be less than one part in 10^3 . In addition, the fields < 5 G were monitored with an optical-pumping Rb magnetometer.⁵⁸ This instrument established a limit of 0.2% on drifts occurring during the experiment. The magnetometer also mapped the field and determined the central-field value.

An independent measurement of all of the relevant properties of the magnetic field was performed by taking data with positive muons. As explained above, precession of both free muon and muonium could be observed in our apparatus. Moreover, since the residual polarization of positive muons is large (~10 times that for negative

TABLE I. Sizes and shapes of the scintillation counters.

Counter	Shape	Thickness (cm)	Length (cm)	Diameter (cm)
S_1	Square	0.16	36	
S_2	Disk	0.16		15
S_3	Disk	0.16		13
S_4	Disk	0.012		13
E_1	Disk	0.6		26
E_2	Disk	0.6		26
E_3	Cylinder	0.6	27	24
E_4	Square	0.6	32	

muons), precise data could be obtained quickly. To produce a positive beam, all of the magnets in the laboratory, the main cyclotron magnet, the channel magnets, and our Helmholtz coils were reversed. This operation could be performed in about an hour, and was done several times during the course of the experiment. Field maps indicated that this operation yielded a field 150 mG ($\sim 3\%$) less for the positive beam and changed slightly the direction but not the magnitude of the spatial nonuniformity of the field. Thus the positive muon and muonium precession frequencies gave independent measures of the average fields (except for the $\sim 3\%$ correction just noted) and the depolarization, as a function of the lifetime of the individual muons gave an empirical check of the effect of the field inhomogeneity (see Sec. VD) and also possible depolarization due to impurity atoms.

D. Counters

All particle detectors were plastic scintillation counters, the dimensions of which are given in Table I. Incoming muons were defined by four counters: S_1 covering the last quadrupole of the muon channel; S_2 in front of the pressure vessel; and S_3 and S_4 inside the pressure vessel. Figure 4 shows their positions. The active region of the target was a cylinder bounded by E_1 which was disk shaped and E_3 which was cylindrical. These served as anticounters for the detection of a stopping muon (μ_s). They were also part of the two telescopes which detected decay electrons. Forward electrons (e_F) were defined by E_1 and E_2 , and downward electrons (e_D) by E_3 and E_4 .

The target gas was only about 55 mg/cm² thick and stopped only a small fraction of the incoming beam. It was therefore critical that the counters be very efficient in rejecting those muons that stopped elsewhere. For example, the thickness of S_4 and any inefficient layer in front of E_1 and E_3 had to be small. These counters were left uncovered because light-tight material would have added to background wall stops. Counter S_4 was

only 0.012 cm thick and was backed with 0.16 cm of lucite to aid in light collection. The effectiveness of the counters in rejecting unwanted muons was measured by counting muon stops with the pressure vessel evacuated. The target empty rate was 25% of the target full rate, corresponding to 18 mg/cm² of scintillation plastic. Subtracting the 12 mg/cm² contribution of S_4 , we find a reasonable figure of 6 mg/cm² for the inefficient layer of E_1 and E_3 . The light output from a muon stopping in 6 mg/cm² corresponds to 0.5-MeV energy deposited including a small correction for the saturation of light output for plastic scintillators.⁵⁹

Special attention was given to the operation and efficiency of S_4 , the 0.012-cm-thick counter backed with 0.16 cm of lucite. A lower bound for its efficiency (\mathcal{E}) could be measured by determining the efficiency of S_4 for muons stopping in E_1

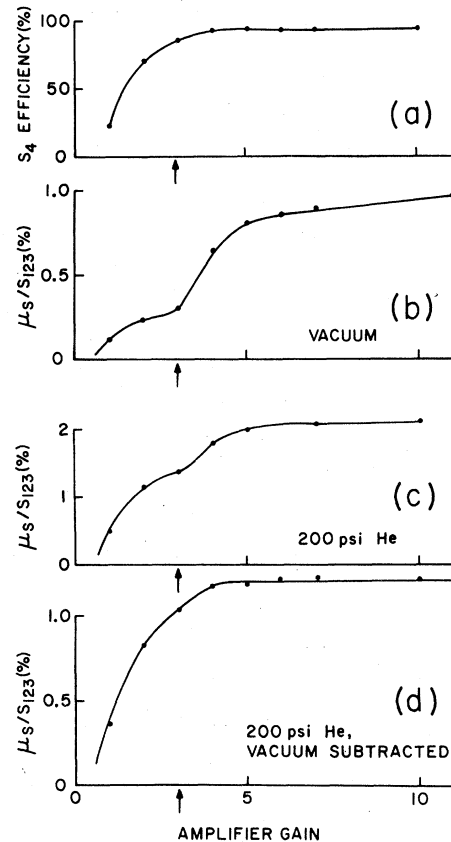


FIG. 6. Study of efficiency of counter S_4 for stopping muons as a function of amplifier gain. (a) Muons stopping in counter E_1 . (b) Vacuum data. The muons presumably stopped in S_4 and in inefficient regions of E_1 and E_3 . (c) Target filled with 14-atm He. (d) Difference between (b) and (c), which gives the relative efficiency in the He gas. Arrows indicate the amplifier gain which was used for taking precession data.

$$\mathcal{E} \geq \frac{(S_1 S_2 S_3 E_1 \bar{E}_2 \bar{E}_3) S_4}{S_1 S_2 S_3 E_1 \bar{E}_2 \bar{E}_3}, \quad (4.4)$$

where the overbars denote anticoincidences. The true efficiency should be slightly greater because (1) S_4 did not precisely cover S_3 and there could be a few percent geometrical inefficiencies and (2) Muons stopping in E_1 , especially those stopping near the end of E_1 , have a higher velocity in S_4 and thus deposit less energy. Figure 6(a) is a graph of the efficiency defined by Eq. (4.4) as a function of the gain of an amplifier in front of the S_4 discriminator. The maximum efficiency is on a wide plateau and equals 96%.

The muon stopping rate ($\mu_s/S_1 S_2 S_3$) with the target evacuated is shown in Fig. 6(b). The striking feature of this graph is the break or change in rate by a factor of 2 between amplifier gains of 3 and 4. Such an effect is unexpected on the basis of the efficiency curve, which shows that with a gain of 3 the counter S_4 is already more than 90% efficient, but is explained as follows. The photomultiplier used, an RCA 8850, has a high-gain gallium-phosphide first dynode and can resolve pulses due to exactly one photoelectron from those due to more than one photoelectron. Below an amplifier gain of 3, one-photoelectron pulses are below the discriminator threshold, but with a gain of 4 or more these small pulses are detected. The break in Fig. 6(b) is associated with one-photoelectron events. These one-photoelectron events are probably muon stops in the 0.16 cm of lucite in front of S_4 . If we assume that lucite scintillates 1000 times less efficiently than scintillator, we would expect an average of $\frac{1}{4}$ photoelectron per muon stop, and there would be enough of these one-photoelectron events to explain the effect.

Further evidence for the above explanation is shown in Figs. 6(c) and 6(d). Figure 6(c) is μ_s versus amplifier gains for the target filled with 14 atm of helium. There is a break which has the same absolute size as the break in the vacuum stop curve [Fig. 6(b)] but a much smaller relative size. Figure 6(d), the difference between Figs. 6(c) and 6(b), represents the S_4 efficiency for true gas stops and looks exactly like the efficiency curve for E_1 stops [Fig. 6(a)].

These μ_s events that are actually due to stops in the lucite are potentially a serious background in that they correspond to 40 mg/cm² of extraneous dead material, a significant fraction of the target material. They are eliminated by operating with an amplifier gain of 3. Under these conditions the efficiency of S_4 is greater than 90%, as indicated by Figs. 6(a) or 6(d), and the target-empty events

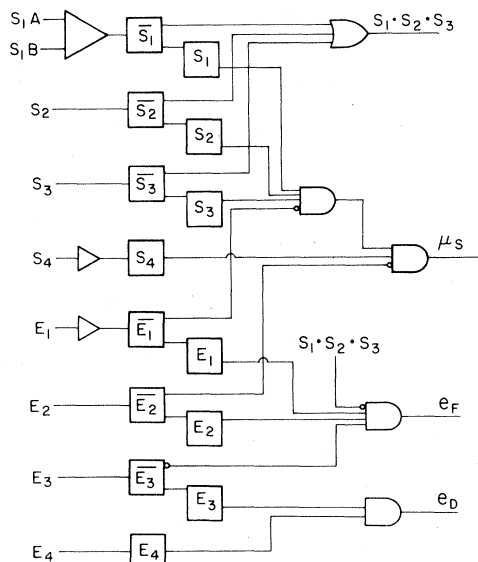


FIG. 7. Block diagram of the fast logic. The large triangle is a linear fan-in; the small triangles are amplifiers; the squares are discriminators; and the coincidence units are given by the usual symbols.

are only 25% of the target-full events. All of the data were taken with an amplifier gain of 3.

E. Logic and data acquisition

The fast logic for the experiment is shown in Fig. 7. A stopping muon (μ_s) is defined by the coincidence $S_1 S_2 S_3 S_4 \bar{E}_1 \bar{E}_2 \bar{E}_3$. With an incident negative muon beam of 3×10^5 /sec at S_1 the μ_s rate was 600/sec with 14-atm He and 150/sec with the target evacuated. Decay electrons were detected as $e_F = E_1 E_2 \bar{S}_1 \bar{S}_2 \bar{S}_3$ and $e_D = E_3 E_4$. One relevant detail of the logic is the fact that the first discriminator of a counter operated in an updating mode and had a relatively long (50-nsec) output pulse suitable for use as an anticounter. Following that discriminator was a second discriminator with a shorter output used for coincidences. The result of this series arrangement was that the coincidence output did not register pulses that caused the anticoincidence to update.

The time intervals between an e_F (or e_D) and a μ_s were obtained with a time-to-amplitude converter (TAC) and a pulse height analyzer (PHA) as shown in Fig. 8. The electron signals were delayed 3μ sec so that accidental electrons counted before the μ_s were recorded and could be used to correct for accidental background.

The blocking logic before the TAC rejected events in which more than one muon was present near the target. Otherwise these events would include a rate-dependent background which would change, among other things, the apparent muon

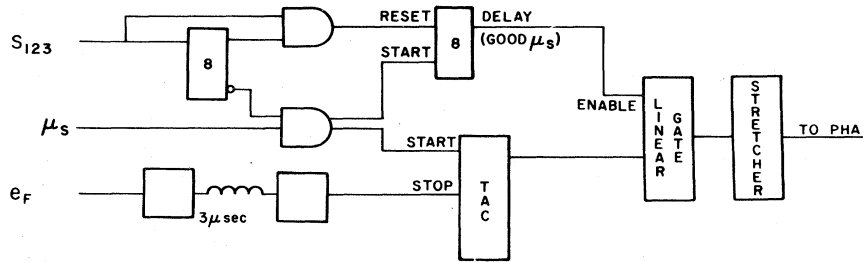


FIG. 8. Block diagram of logic used to select good e_F events and generate a TAC pulse for the PHA.

lifetime. Such effects would complicate the interpretation of the time spectra, especially those with small signals and relatively slow Larmor-precession frequencies. The price of this logic was the loss of a factor of 3 in live time. The blocking logic was important for the e_F signal because the large number of muons which stopped in E_1 had a large solid angle for detection as an e_F and represented a potentially large accidental background rate. For the e_D signal the accidental rate was low, and the simplified logic of Fig. 9 was used. For some of the ${}^4\text{He}\mu^-e^-$ data the blocking logic for e_F was modified as shown in Fig. 10 to increase the live time. This resulted in a complicated but slowly varying background which was not difficult to separate from the relatively fast Larmor precession of the atom.

Four separate TAC's and PHA's were used. The first PHA was a Nuclear Data analyzer which had the advantage that its data could be analyzed by computer software which was ready before the start of the run. Also it was the only analyzer operating throughout the entire experiment. The e_D signal was stored in a Kicksort analyzer. Two more Kicksort ADC's interfaced to an IBM 360 computer at SREL were operational during the latter part of the experiment. They were used for redundant spectra, one for e_F and one for e_D .

All analyzers were frequently calibrated with a 5-MHz time-mark generator. For the two computer analyzers, the time per channel was uniform and stable in time to better than 0.3% and the channel corresponding to $t=0$ drifted by at most 10 nsec. The off-line ND analyzer was linear to 0.5% but had a drift in the $t=0$ channel of as much as 50 nsec over the course of the experiment. This later effect, although of no importance for

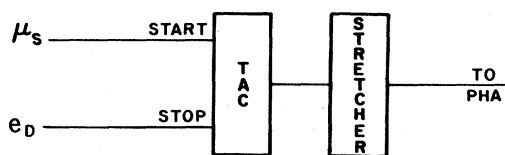


FIG. 9. Logic diagram for the e_D signal.

the slow free precession, would be of some concern for the higher-frequency ${}^4\text{He}\mu^-e^-$ data. However, the more stable computer spectra were available for all of that data.

V. DATA AND ANALYSIS

Four different groups of data were taken:

Group I. Search for precession of $({}^4\text{He}\mu^-)^*$ at 67 G. Data were taken mainly with the e_F telescope. Targets used were pure helium, helium plus xenon, and vacuum.

Group II. Search for ${}^4\text{He}\mu^-e^-$. Magnetic fields of 3.10 and 3.73 G were used. Both e_F and e_D telescopes collected data. The target was 14-atm helium plus 2% xenon.

Group III. Search for ${}^4\text{He}\mu^-e^-$. Same as Group II except that magnetic fields of 3.42 and 4.64 G were used, and the alternate slow logic (Fig. 10) was used for the e_F spectra.

Group IV. Positive muon studies. Data with positive muons in the He-Xe mixture for Groups II and III and also in various other noble gases were obtained and used to calibrate the apparatus and measure its analyzing power so that absolute residual polarizations could be calculated.

A. Calibration with μ^+ data

The fourth group of data, taken with positive muons, was the simplest to analyze because the large precession amplitudes were clearly visible in the raw time spectra. Figure 11 shows typical spectra for μ^+ stopped in 7 atm of pure helium at a magnetic field of 67 G. Both e_F and e_D signals are shown. The oscillations due to free muon precession are the dominant feature. An e_D spectrum for μ^+ stopped in 14-atm helium plus 2% Xe at 3.63 G is shown in Fig. 12. The more rapid

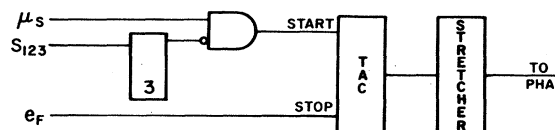


FIG. 10. Modified logic for e_F .

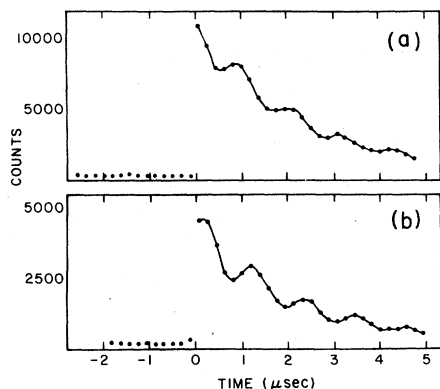


FIG. 11. Time spectra for positive muons stopped in pure helium for (a) e_F and (b) e_D . The precession is due to a magnetic field of 67 G. The 90° phase difference and the difference in precession amplitude between the two spectra are readily visible.

muonium precession is readily visible. The oscillations are seen to disappear after about $2 \mu\text{sec}$ as expected due to the nonuniformity of the magnetic field.

From this positive muon data it was possible to extract empirical values a^μ or a^M , the analyzing power of the system defined by Eq. (2.14). The value of a depends upon many factors; among the more important are beam polarization, solid angle acceptance of the electron telescope, energy spectrum of electrons detected by the telescope, and of course the fraction of muons that remain as free muons and the fraction that form muonium.⁶⁰ Values for a for both telescopes, and for muonium and for free muon precession, are given in Table II. These numbers are based on data for positive muons stopped in He and He-Xe mixtures, some of which are shown in Figs. 11 and 12, respectively, and also on Ar and Kr data. This analysis assumed that all positive muons either precess as free muons or form muonium. The quoted errors include a systematic contribution estimated by comparing different gases with different pressures. We will assume that the ana-

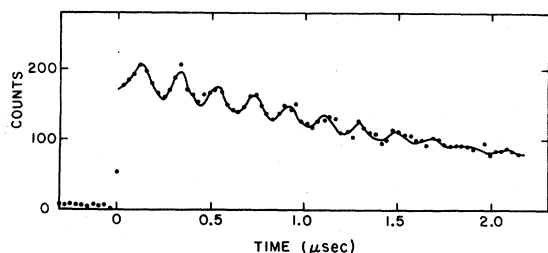


FIG. 12. Time spectrum for μ^+ stopped in 14-atm He plus 2% Xe at 3.73 G. The precession of the muonium formed is apparent. Data are for the e_D telescope.

TABLE II. Values of calibration constants required to extract the absolute polarization of the $({}^4\text{He}\mu^-)^*$ and ${}^4\text{He}\mu^-e^-$ from raw precession amplitudes.

Symbol	Telescope	Maximum asymmetry parameter (a)	
		Free muons or muonium	a (%)
a_F^H	e_F	free	19 ± 1
a_F^M	e_F	muonium	9.5 ± 0.5
a_D^H	e_D	free	30 ± 1
a_D^M	e_D	muonium	15.0 ± 0.5

Fraction of wall stops (α)	
Pressure (atm He)	α (%)
7	33 ± 3
14	20 ± 2

lyzing power for positive and negative muons is the same, apart from the depolarizing effects for negative muons which we are studying.

An interesting feature of Table II is the fact that the analyzing powers of the e_F and e_D telescopes differ substantially. This effect is caused by the 5-cm-thick pressure vessel wall which absorbs the low-energy electrons in the e_D telescope. The low-energy electrons emitted in muon decay have a negative analyzing power,⁶¹ and their absorption results in a higher overall analyzing power.

B. Special features of the μ^- data

The raw data for negative muons ideally should have no readily visible features other than the flat background plus the exponential decay as shown in Fig. 13(a). The amplitude of any oscillations present is too small to be readily apparent in a

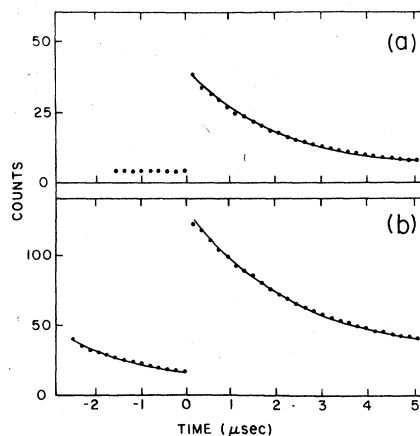


FIG. 13. Typical spectra for negative muons. (a) Telescope e_D . (b) Telescope e_F with logic of Fig. 10.

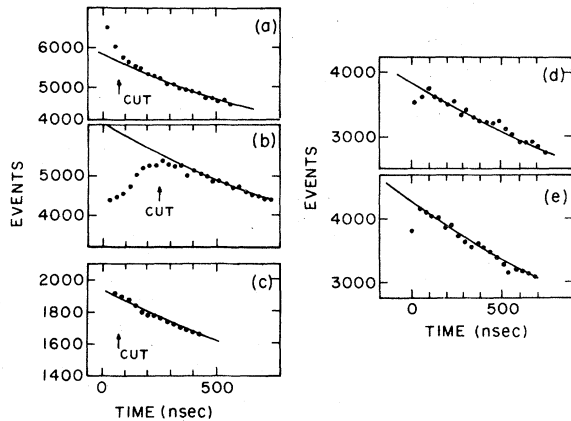


FIG. 14. Detail of time spectra near $t=0$ for negative muons. (a) Spike due to Xe capture as exhibited by e_D . (b) Dip appearing in e_F spectra with 2% Xe admixture and before electronics adjustment. (c) Same as (b) but after electronics were adjusted to reject single photoelectrons. (d) Data for e_F with 1.2% Xe. (e) Data for e_F with pure helium.

single run. An exception is the e_F signal for Group III, an example of which is shown in Fig. 13(b). These spectra are the only ones in which the slow logic was changed to the configuration in Fig. 10. The time dependence of the negative time data is due to the short 3- μ sec blocking of that logic. This data also yielded a longer apparent muon lifetime. With the normal logic of Fig. 8, the negative time background was flat, and the spectra looked like the typical e_D spectrum shown in Fig. 13(a).

The addition of Xe to the helium changed the shape of the spectra for times near zero. One effect, shown for e_D in Fig. 14(a) is the presence of a second lifetime equal to $\approx 0.1 \mu$ sec. This is the lifetime for negative muons captured by Xe,⁶² and the size of this "spike" is consistent with the predictions of the Z law for muon capture in compound materials.

A much more curious effect is seen in Fig. 14(b), which is the e_F spectrum for the same run displayed in Fig. 14(a). Here there is a dip for short time instead of a spike, but with a comparable decay time of ≈ 100 nsec. The cause of this dip is possibly slow scintillations from the target gas which were counted by E_1 . Using the same apparatus, we observed that for positive muons stopping in pure Kr and Xe only about half as many μ_s were observed as were expected on the basis of the stopping power and densities of the gas. The other noble gases, He, Ne, and Ar, yielded expected stopping rates. Kr and Xe apparently produced sufficient prompt scintillation light to be detected by E_1 functioning as an anti-

counter for μ_s . Since the target gas was able to scintillate sufficiently to veto good stops, it seems reasonable to explain the dip by metastable states in the gas with a lifetime of ~ 100 nsec. Their decay could trigger E_1 and cause time-dependent dead time in the e_F logic, due to the updating feature, with a 100-nsec time constant. Electrons traversing E_1 during this time would thus have a smaller probability for being detected.

The above explanation implies that the dip is due to single photoelectrons. Counter E_3 , which had an RCA 8850 photomultiplier like the one on S_4 , was operated such that at least two photoelectrons had to be collected to trigger the discriminator. This explains why the e_D spectra, which use counter E_3 but not E_1 , showed no dip. For the third data group (3.42 and 4.64 G) the logic was changed slightly so that single photoelectrons could not cause dead time in the e_F telescopes. The result, shown in Fig. 14(c), was that the dip was eliminated.

For comparison, data with 1.2% Xe and with 0% Xe in the helium are shown in Figs. 14(d) and 14(e), respectively. There is no dip or spike in pure helium. However, the 1.2%-Xe data, with more than half of the Xe as the 2%-Xe data, shows almost no dip. This effect is not understood but is not important for this experiment since those regions of the spectra were cut.

C. Free-precession data

The data from Group I were used to study the residual polarization of negative muons in helium by searching for a free muon Larmor-precession signal. The dips and spikes of data Groups II and III were not present and did not need to be accounted for in the analysis. The data from Group I were obtained with pure He at 7 and 14 atm and also with the target evacuated. In addition, data were taken with Xe admixtures of 0.2%, 1.2%, and 2%. A magnetic field of 67 G was used for most of the data, although some were taken at 3.7 G and provided useful checks. The time distributions of the data were fitted with the equation

$$N(t) = N_0 \exp(-t/\tau) \times [1 + A_R \exp(-t/\tau_D) \cos(2\pi ft + \phi)] + B + Ct, \quad (5.1)$$

where $N(t)$ is the observed number of events at time t (an event is an e_F or e_D count occurring at a time t after a muon stop), N_0 is a normalization constant, τ is the muon lifetime, τ_D is a depolarization time constant, A_R is the raw precession amplitude, $f = \gamma H$ is the precession frequency, ϕ is the initial phase, and B and C are background parameters. For negative times N_0 was set to

zero so that only B and C contributed.

Trial fits were made with all parameters free to vary, including τ , τ_D , and f . Best fits were obtained where τ was consistent with the known muon lifetime of $2.2 \mu\text{sec}$ and τ_D was consistent with infinity. The one exception is the vacuum data in which the best lifetime was $2.0 \mu\text{sec}$, consistent with the accepted value for μ^- stopped in carbon.⁶² The first 230 nsec after the μ_s were not used in the final fits to avoid any possible problem due to the spikes and dips discussed above. The results are insensitive to the exact size of this cut.

The results are displayed by plotting A_R as a function of f or equivalently as a function of $\gamma = f/H$. Such graphs are called gyromagnetic ratio plots. For this analysis the parameters τ and τ_D and ϕ are fixed at their expected values of $\tau = 2.2 \mu\text{sec}$, $\tau_D = \infty$, and $\phi = 0$. Figure 15(a) shows a gyromagnetic ratio plot for the μ^+ data whose raw spectrum was given in Fig. 11. The corresponding plot for μ^- stopped in 14-atm He is shown in Fig. 15(b). There is a clear signal at the correct gyromagnetic ratio and with the same shape as the μ^+ data. Gyromagnetic ratio plots for other target conditions are also given in Fig. 15. A complete tabulation of the A_R values obtained with τ , τ_D , and f all fixed at their expected values is given in Table III.

The amplitude A due to muons stopping in the gas is obtained from the raw amplitude A_R , and the amplitude from the vacuum or target-empty data A_V , together with the equation

$$A_R = \alpha A_V + (1 - \alpha)A \quad (5.2)$$

The phase angle ϕ is set to its expected value of 0 for this analysis. We note that this is equivalent to multiplying A_R by $\cos\phi$. The parameter α is the fraction of detected electrons coming from

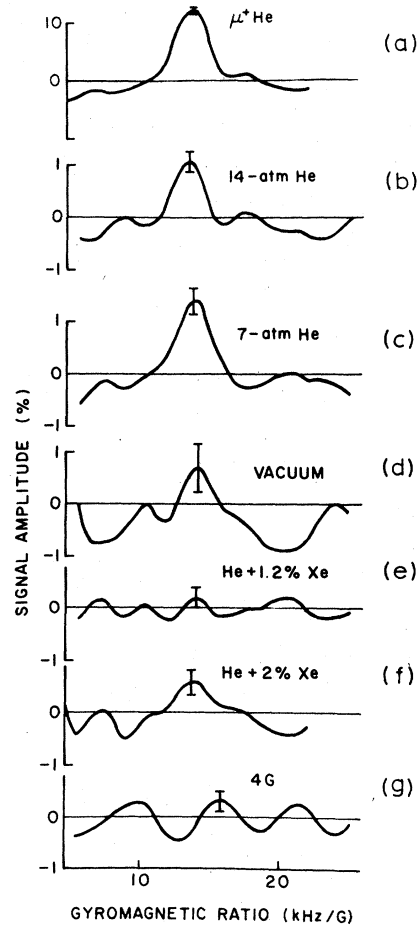


FIG. 15. Gyromagnetic ratio plots used to study $({}^4\text{He}\mu^-e^-)^+$ precession at 67 G. (a) Positive muons stopped in pure He serve as a calibration. Negative muons were stopped in (b) 14-atm He, (c) 7-atm He, (d) Vacuum, (e) 14-atm He plus 1.2% Xe, and (f) 14-atm He plus 2% Xe. (g) Systematic error study with data obtained at 4 G but analyzed exactly like the 67-G data. Pure He at 14 atm was used.

TABLE III. Results of data analysis for the residual polarization of $({}^4\text{He}\mu^-)^+$. The predicted frequency for 67 G (0.91 MHz) is used for all the data.

Data group	He pressure (atm)	Xe (%)	B (G)	Number of μ_s (10^4)	A_R^a (%)	ϕ (radian)	A^b (%)	P^μ (%)
1	14	0	67	3.6	1.02 ± 0.17	0.14	1.11 ± 0.24	5.8 ± 1.3
2	7	0	67	1.6	1.42 ± 0.24	0.06	1.79 ± 0.42	9.4 ± 2.3
3	0	0	67	0.8	0.67 ± 0.45	0.07		
4	14	0.2	67	1.9	1.19 ± 0.21	0.26	1.27 ± 0.29	6.7 ± 1.6
5	14	1.2	67	2.6	0.22 ± 0.20	-0.46	$+0.08 \pm 0.28$	0.4 ± 1.6
6	14	2.0	67	1.9	0.60 ± 0.25	-0.24	0.56 ± 0.33	2.9 ± 1.8
7	14	0	4	1.0	0.39 ± 0.27	-2.08	-0.19 ± 0.27	
8	14	1.2	4	3.3	0.40 ± 0.18	-2.56	-0.34 ± 0.18	

^a Raw amplitude.

^b Amplitude corrected for vacuum stops.

muons which stopped in the walls. Values for α at different pressures are given in Table II. They were measured by comparing rates for target-full and target-empty data. The ratio of μ_s for target full versus target empty, which is 25% at 14 atm, is slightly larger than α (20% under the same condition) because the telescopes had a smaller solid angle for wall stops.

The absolute residual polarization P^μ was calculated from the formula

$$P^\mu = A/a^\mu, \quad (5.3)$$

where A is defined in Eq. (5.2) and a^μ is the analyzing power of the telescope as given in Table II. Final values for A and P^μ for all of the target conditions are given in Table III. Small differences between these results and those published earlier² are due to including slightly more data and changing the starting time cut to 230 nsec.

In pure He at pressures of both 7 and 14 atm there is a statistically significant nonzero value for the residual polarization. The only potentially important correction is the contribution due to the wall stops. However, this correction is small and should be reliable because the width of the μ^- stopping distribution in g/cm² is large compared to the thickness of the He. The value of the residual polarization in pure helium is smaller by a factor of 3 compared to the predictions of the conventional theory of cascade depolarization. The amplitude for the 7-atm data is somewhat larger than that for 14 atm, but the errors are too large to draw a definite conclusion.

Adding 0.2% Xe to the helium had no observable effect on the free-muon precession. The results of adding more Xe show that the free-muon amplitude is greatly reduced. The 1.2%-Xe data shows no signal, and for 2% Xe there is only a small signal of less than two standard deviations.

The residual polarization for the vacuum data is consistent with published values for μ^- stopped in polystyrene.⁶³ This fact gives us further confidence that our wall-stop corrections are reliable. The data taken at 3.7 G showed no signal at the frequency expected at 67 G.

D. Search for ${}^4\text{He}\mu^-e^-$

In view of the nonzero residual polarization of μ^- stopped in helium and the quenching effect of the added Xe, we took Data Groups II and III to search for the characteristic ${}^4\text{He}\mu^-e^-$ precession. An admixture of 2% was used. The ${}^4\text{He}\mu^-e^-$ data were analyzed with a more complicated equation which accounted for

- (1) the "spike" due to muons captured by the Xe or the curious dip described above, and
- (2) the nonuniformity of the magnetic field which

resulted in significant depolarization after a few μsec .

The equation used was

$$N(t) = N_0 \exp(-t/\tau) \times \{1 + A_R [\sin(2\pi\gamma\Delta H t) / 2\pi\gamma\Delta H t] \cos(2\pi f t + \phi)\} + B + C t + D \exp(-t/\tau_x), \quad (5.4)$$

where ΔH is the nonuniformity of the magnetic field, τ_x is the muon lifetime in Xe or a decay parameter for the dip, D is a normalization constant, and the other parameters are the same as for Eq. (5.1). A theoretical value of $\Delta H = 0.14$ G is derived from the measured nonuniformity of the magnet. We found that a value of 0.15 G for ΔH yielded the best fits, in good agreement with the above prediction. In order to minimize the sensitivity of the fitted amplitudes to the depolarization parameter ΔH , the spectra were cut off for times greater than $(\pi\gamma\Delta H)^{-1} = 1.6 \mu\text{sec}$, corresponding to a depolarization of 0.45. For the two groups of data analyzed here, both e_F and e_D spectra were available.

Approximately equal amounts of data were taken at each of four different magnetic fields: 3.10, 3.42, 3.73, and 4.64 G. A total of $3 \times 10^8 \mu_s$ were obtained for this part of the experiment. Since data from two telescopes were available at each field, there were eight sets of data to analyze. The results for each set are given in Table IV. The raw amplitudes were calculated for fixed values of ϕ , 0 for e_F , and $-\pi/2$ for e_D , which were confirmed by muonium data.

In Fig. 16 the four e_D spectra are analyzed individually as a function of frequency. Here one can see that the signals are correlated with the magnetic field. The method of using different magnetic fields eliminates systematic errors such as a periodic differential nonlinearity in the pulse-height analyzers. The small negative amplitude at 7.4 MHz for each spectrum could be due to this effect.

All of the data taken at the four magnetic field values were combined by calculating the amplitude A_R as a function of gyromagnetic ratio. The result for the e_F and e_D spectra are shown in Fig. 17. Both signals, which are statistically independent, show a clear peak at $\gamma = 1.4$ MHz/G. For comparison, the figures also show muonium data taken under identical conditions except for beam polarity as explained in Sec. V C. The width of all of the peaks at $\gamma = 1.4$ MHz/G are the same. The difference in analyzing power between the two telescopes is also apparent. We thus conclude that polarized ${}^4\text{He}\mu^-e^-$ atoms were formed.

We could successfully combine the data in the above fashion only because we independently es-

TABLE IV. Summary of analysis of ${}^4\text{He}\mu^-e^-$ data for each magnetic field and for each telescope.

Signal	e_F	e_F	e_F	e_F	e_D	e_D	e_D	e_D
B(G)	3.10	3.42	3.73	4.64	3.10	3.42	3.73	4.64
Time analyzed (μsec)	0.25- 1.53	0.12- 1.53	0.23- 1.53	0.12- 1.53	0.07- 1.47	0.07- 1.47	0.07- 1.47	0.07- 1.47
τ (μsec)	2.15	2.9	2.18	2.9	2.19	2.19	2.16	2.15
τ_x (nsec)	98	89	94	100	77	91	80	71
$\frac{\chi^2}{\text{DF}}^a$	$\frac{297}{284}$	$\frac{247}{194}$	$\frac{348}{337}$	$\frac{314}{194}$	$\frac{351}{361}$	$\frac{393}{361}$	$\frac{369}{361}$	$\frac{428}{361}$
A_R (%)	0.68 ± 0.23	0.36 ± 0.12	-0.15 ± 0.22	0.38 ± 0.12	0.72 ± 0.24	0.49 ± 0.21	0.89 ± 0.23	0.61 ± 0.21

^a Degrees of freedom.

established values for H (see Sec. IV C) and ϕ . If the several values of H were measured incorrectly, the peaks in Fig. 17 would be broadened and suffer a corresponding loss in height. If ϕ were left as a free parameter, A_R would become a quantity constrained to be non-negative. With

our statistics, the distribution of A_R values would then become skewed, not centered on the expected value and rather insensitive to the expected value.

The amplitudes due to the gas, A of Eq. (5.2), were obtained from Eq. (5.2) with the reasonable assumption that muons stopping in the counters do not precess at the ${}^4\text{He}\mu^-e^-$ frequency and that therefore $A_V = 0$. The parameter α in that equation is the same as was used for the free-precession data. The contribution to the residual polari-

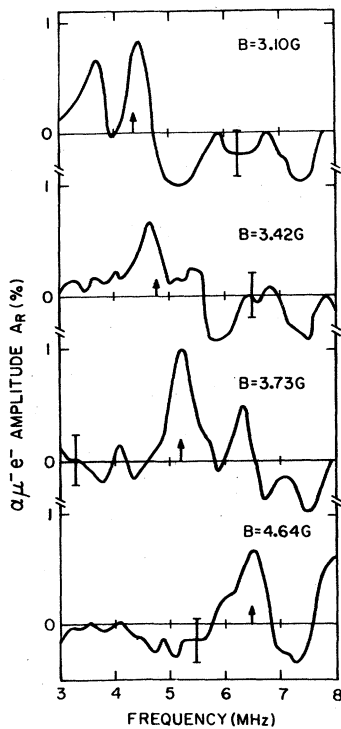


FIG. 16. Raw amplitude A_R as a function of frequency f for negative muons stopped in 14-atm He plus 2% Xe for different magnetic-field values. Data are for the e_D telescope. Arrows indicate the expected frequency for the ${}^4\text{He}\mu^-e^-$ signal.

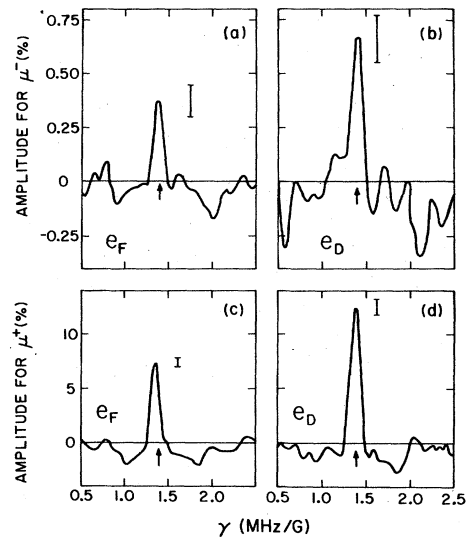


FIG. 17. Observed Larmor-precession amplitude A_R versus gyromagnetic ratio $\gamma = f/H$: (a) and (b) μ^- stopped in He+2% Xe and forming ${}^4\text{He}\mu^-e^-$; (c) and (d) μ^+ stopped in He+2% Xe and forming ${}^4\text{He}\mu^+e^-$. Data for (a) and (c) were obtained with electron telescope e_F , and data for (b) and (d) were obtained with e_D . Results from the two telescopes are statistically independent. The arrows indicate the expected gyromagnetic ratio $\gamma = 1.4$ MHz/G.

zation detected through the muonic-helium-atom precession was calculated with the equation

$$P^M = A/a^M, \quad (5.5)$$

where the values for a^M are given in Table II. Final results for A and P^M appear in Table V.

The total residual polarization P_T is the sum of the free muon contribution P^μ and P^M , the contribution from the atom. Our measurements of P_T for different pressures and Xe admixtures are summarized in Table VI. It is assumed that no significant ${}^4\text{He}\mu^-e^-$ formation occurs except for the case where 2% Xe was added.

VI. DISCUSSION AND CONCLUSIONS

In this experiment we have made the first observation of a nonzero signal for the precession of the spins of negative muons stopped in helium. As our primary goal, we have also demonstrated the formation of polarized muonic helium atoms when negative muons are stopped in a gas mixture of helium and a small amount (2%) of Xe. The residual polarization for both of these systems, however, is a factor of 2 to 3 smaller than predicted by the simple cascade-depolarization theory. We have hypothesized that collisions of the $({}^4\text{He}\mu^-)^+$ ion while it is highly excited are responsible for this additional depolarization. More detailed theoretical calculation on this problem would be very useful.

From our results we can extract some information about the various reactions that are important for the neutralization of the muonic helium ion to form its atom. The facts that 0.2% Xe has little effect on the free-precession signal and that 2% Xe results in the copious formation of ${}^4\text{He}\mu^-e^-$ in phase do support the hypothesis that molecular ions or even clusters are formed. The fact that 2% Xe forms ${}^4\text{He}\mu^-e^-$ rapidly compared to the precession period (otherwise the atoms would dephase and no signal could be seen) does establish a lower bound to the Xe cross section of $\sigma > 10^{-17}$

TABLE V. Amplitudes and residual polarizations for e_F and e_D obtained by averaging data from all four magnetic-field values.

Electron telescope	e_F	e_D
Raw amplitude (A_R) (%)	0.342 ± 0.075	0.66 ± 0.11
A (corrected for wall stops) (%)	0.42 ± 0.09	0.83 ± 0.14
P (residual polarization exhibited by $\alpha\mu^-e^-$) (%)	4.4 ± 1.0	5.5 ± 0.9
P (final average)	5.0 ± 0.7	

cm^2 . In turn, this limit requires that the molecular-ion formation rate constant $\lambda({}^4\text{He}^-)/n^2$ be larger than $6 \times 10^{-36} \text{ cm}^2/\text{sec}$. These numbers, although not very restrictive, are consistent with our estimates.

Techniques similar to those of this experiment could be used to extract additional information about the above reactions. For example, detailed measurements of the free muon and ${}^4\text{He}\mu^-e^-$ precession amplitudes as a function of Xe concentration and of helium pressure should reveal the quadratic pressure dependence of molecular-ion formation and verify that this reaction is indeed important. Of course, a good understanding of the pressure dependence of the residual polarization is a prerequisite. This is in contrast to muonium, where the pressure dependence is not a good test of molecular-ion formation because of the likely difference in energies where the two reactions occur. Presumably all relevant interactions of $({}^4\text{He}\mu^-)^+$ occur at thermal energy. Also, studies of other electron donors which have large charge-transfer cross sections at thermal energies (perhaps CH_4 or C_2H_6) would be interesting.

The ability to produce polarized ${}^4\text{He}\mu^-e^-$ atoms allows the hyperfine structure interval to be measured by the same microwave resonance techniques that have been applied to muonium.^{60,64-66} Since the signal amplitudes are proportional to the residual polarization of the atoms, the muonic helium atom with its 5% polarization is a more difficult system to study than muonium. However, experiments are in progress at the Schweizerisches Institut für Nuklearforschung (SIN)⁶⁷ and the Clinton P. Anderson Meson Physics Facility (LAMPF),⁶⁸ and preliminary data indicate that resonance signals are being observed at both laboratories.⁶⁹

At present a precision measurement of $\Delta\nu$ for the muonic helium atom is of greatest interest as a test of the theory of the atom's structure. The precise calculation of the wave function for an atom with three particles is a fundamental problem in quantum mechanics; the ${}^4\text{He}\mu^-e^-$ atom is unusual since the three particles have unequal

TABLE VI. Total residual polarizations.

He pressure (atm)	Xe (%)	P^μ (%)	P^M (%)	P_{total} (%)
7	0	9.4 ± 2.3	0 ^a	9.4 ± 2.3
14	0	5.8 ± 1.3	0 ^a	5.8 ± 1.3
14	0.2	6.7 ± 1.6	0 ^a	6.7 ± 1.6
14	2.0	2.9 ± 1.8	5.0 ± 0.7	7.9 ± 1.9

^a Assumed values.

masses. Since the atom is in principle a simple, purely electromagnetic system (the nuclear structure of the alpha particle does not play a significant role in the calculations), better calculations are very desirable.

Since the atomic structure can in principle be known to very high precision, it is interesting to consider what can be learned about the fundamental negative muon-electron interaction by studying this atom. It is convenient to make a comparison with $\Delta\nu$ for muonium, which has already been measured very accurately. If $\Delta\nu$ is measured for both ${}^4\text{He}\mu^-e^-$ and muonium, then the ratio

$$R \equiv \frac{\Delta\nu(\text{muonium})}{\Delta\nu({}^4\text{He}\mu^-e^-)} \quad (6.1)$$

can be determined. The fundamental constants required for the calculations, including μ_μ and α , cancel in R to first order. If CPT is not conserved and the magnetic moments for μ^+ and μ^- are different,⁷⁰ R will be changed. The contribution to $\Delta\nu$ from weak neutral currents, in particular an axial-electron axial-muon coupling,⁷¹ will change R . In the Weinberg-Salam model⁷² the correction to R is 0.03 ppm and in a $\text{SU}(2) \times \text{SU}(2)$

$\times \text{U}(1)$ model⁷³ the correction is 0.06 ppm. The present experimental error on $\Delta\nu$ for muonium is 0.12 ppm,⁶⁵ not very much larger than the weak-interaction corrections. The uncertainty from uncalculated quantum-electrodynamics terms for muonium (0.5 ppm)⁷⁴ is larger than the experimental uncertainty and the present calculation for ${}^4\text{He}\mu^-e^-$ is much less precise. Nevertheless, we feel that the level of precision required to see the weak-interaction effects is an appropriate, although ambitious, goal for future theoretical and experimental studies.

ACKNOWLEDGMENT

We are happy to acknowledge the enthusiastic and effective support of Professor Robert Siegel of the College of William and Mary, who was Director of the Space Radiation Effects Laboratory where our experiment was done. This research was supported in part by the U. S. Department of Energy under Contract No. EY-76-C-02-3075. H. W. Reist is a recipient of a fellowship from the Schweizerisches Institut für Nuklearforschung.

*Present address: Los Alamos Scientific Laboratory, Los Alamos, New Mexico.

†On leave from the University of Heidelberg, Heidelberg, Germany.

‡On leave from the University of Bern, Bern, Switzerland. Present address: Eidgenössisches Institut für Reaktorforschung, Würenlingen, Switzerland.

¹In this paper ${}^4\text{He}$ refers to the helium nucleus. He refers to the helium atom.

²P. A. Souder *et al.*, Phys. Rev. Lett. **34**, 1417 (1975).

³V. G. Varlamov *et al.*, Zh. Eksp. Teor. Fiz. Pis'ma Red. **17**, 186 (1973) [JETP Lett. **17**, 132 (1973)].

⁴V. G. Varlamov *et al.*, Yad. Fiz. **21**, 120 (1975) [Sov. J. Nucl. Phys. **21**, 61 (1975)].

⁵V. W. Hughes and S. Penman, Bull. Am. Phys. Soc. **4**, 80 (1957)

⁶E. W. Otten, Z. Phys. **225**, 393 (1969).

⁷K. N. Huang *et al.*, in *Proceedings of the Fifth International Conference on High Energy Physics and Nuclear Structure*, edited by G. Tibell (North-Holland, Amsterdam, 1973), p. 312.

⁸A. Bohr, Phys. Rev. **73**, 1109 (1948).

⁹J. E. Nafe and E. B. Nelson, Phys. Rev. **73**, 718 (1948).

¹⁰K. N. Huang, Ph.D. thesis, Yale University, 1974 (unpublished).

¹¹K. N. Huang and V. W. Hughes, Phys. Rev. A **20**, 706 (1979).

¹²S. D. Lakdawala and P. J. Mohr (private communication).

¹³E. Borie, Z. Phys. A **291**, 107 (1979).

¹⁴G. Breit, Nature (London) **122**, 649 (1928).

¹⁵W. E. Lamb, Jr., Phys. Rev. **60**, 817 (1941).

¹⁶R. S. Van Dyck *et al.*, Phys. Rev. Lett. **38**, 310 (1977).

¹⁷J. Bailey *et al.*, Phys. Lett. **67B**, 225 (1977).

¹⁸G. Breit and I. I. Rabi, Phys. Rev. **38**, 2082 (1931).

¹⁹P. Kusch and V. W. Hughes, *Encyclopedia of Physics*, edited by S. Flugge (Springer, Berlin, 1959), Vol. 37/1, p. 1.

²⁰V. W. Hughes *et al.*, Phys. Rev. A **1**, 595 (1970).

²¹V. W. Hughes *et al.*, Phys. Rev. Lett. **5**, 63 (1960).

²²R. L. Garwin *et al.*, Phys. Rev. **105**, 1415 (1957).

²³V. S. Evseev, in *Muon Physics*, edited by V. W. Hughes and C. S. Wu (Academic, New York, 1975), Vol. 3, p. 236.

²⁴L. I. Ponomarev, Annu. Rev. Nucl. Sci. **23**, 395 (1973).

²⁵E. H. S. Burhop, in *High Energy Physics*, edited by E. H. S. Burhop (Academic, New York, 1969), Vol. 3, p. 109ff.

²⁶R. A. Mann and M. E. Rose, Phys. Rev. **121**, 293 (1961).

²⁷G. R. Burbidge *et al.*, Phys. Rev. **89**, 189 (1953).

²⁸I. M. Shmushkevich, Nucl. Phys. **11**, 419 (1959).

²⁹A. E. Ignatenko *et al.*, Zh. Eksp. Teor. Fiz. **35**, 1131 (1958) [Sov. Phys.—JETP **8**, 792 (1958)].

³⁰A. Astbury *et al.*, Proc. Phys. Soc. London **78**, 1144 (1961).

³¹V. W. Hughes *et al.*, Bull. Am. Phys. Soc. **5**, 75 (1960).

³²D. C. Buckle *et al.*, Phys. Rev. Lett. **20**, 705 (1968).

³³P. A. Souder *et al.*, in *Proceedings of the Fourth International Conference on Atomic Physics, Heidelberg, Germany, 1974, Abstracts of Contributed Pa-*

- pers*, edited by J. Kowalski and H. G. Weber (Heidelberg University Press, Heidelberg, Germany, 1974), p. 32.
- ³⁴T. B. Day, *Nuovo Cimento* **18**, 381 (1960); T. B. Day *et al.*, *Phys. Rev. Lett.* **5**, 112 (1960).
- ³⁵O. A. Zaimidoroga *et al.*, *Zh. Eksp. Teor. Fiz.* **52**, 97 (1967) [*Sov. Phys.—JETP* **25**, 63 (1967)].
- ³⁶A. Placci *et al.*, *Nuovo Cimento* **1A**, 445 (1971).
- ³⁷A. Bertin *et al.*, *Nuovo Cimento* **26B**, 433 (1975).
- ³⁸W. Happer, *Rev. Mod. Phys.* **44**, 169 (1972).
- ³⁹M. J. D'yakonov and V. I. Perel', *Zh. Eksp. Teor. Fiz.* **47**, 1483 (1964) [*Sov. Phys.—JETP* **20**, 997 (1965)].
- ⁴⁰A. Omont, *J. Phys. (Paris)* **26**, 26 (1965).
- ⁴¹A. T. Okunevich and V. I. Perel', *Zh. Eksp. Teor. Fiz.* **58**, 666 (1970) [*Sov. Phys.—JETP* **31**, 356 (1970)].
- ⁴²E. W. Weber *et al.*, *Z. Phys.* **260**, 341 (1973).
- ⁴³V. W. Hughes, *Phys. Rev.* **108**, 1106 (1957).
- ⁴⁴G. Carboni and O. Pitzurra, *Nuovo Cimento* **25B**, 367 (1975).
- ⁴⁵R. O. Mueller *et al.*, *Phys. Rev. A* **11**, 1175 (1975).
- ⁴⁶M. Camani, *Helv. Phys. Acta* **46**, 47 (1973).
- ⁴⁷W. B. Meier II, *Phys. Rev. A* **5**, 1256 (1972).
- ⁴⁸H. S. W. Massey and E. H. S. Burhop, *Electronic and Ion Impact Phenomena* (Oxford University Press, New York, 1952), p. 450.
- ⁴⁹H. H. Michels *et al.*, *J. Chem. Phys.* **39**, 1464 (1963); A. A. Evett, *ibid.* **24**, 150 (1956).
- ⁵⁰E. C. Beaty and P. L. Patterson, *Phys. Rev.* **137**, A346 (1965).
- ⁵¹R. D. Stambaugh *et al.*, *Phys. Rev. Lett.* **33**, 568 (1974).
- ⁵²R. D. Stambaugh, Ph.D. thesis, Yale University, 1974 (unpublished).
- ⁵³E. Fermi and E. Teller, *Phys. Rev.* **72**, 399 (1947).
- ⁵⁴Yu. G. Budyashov *et al.*, *Yad. Fiz.* **5**, 830 (1967) [*Sov. J. Nucl. Phys.* **5**, 589 (1967)].
- ⁵⁵P. A. Thompson *et al.*, *Phys. Rev. A* **8**, 86 (1973).
- ⁵⁶Matheson-grade helium, Matheson Gas Products, East Rutherford, N. J.
- ⁵⁷Research-grade Xenon, Air Products and Chemicals, Inc., Emmaus, Pa.
- ⁵⁸W. Farr and E. W. Otten, *Appl. Phys.* **3**, 367 (1974).
- ⁵⁹J. B. Birks, *Scintillation Counters* (Pergamon, New York, 1960).
- ⁶⁰J. M. Bailey *et al.*, *Phys. Rev. A* **3**, 871 (1971).
- ⁶¹W. E. Cleland *et al.*, *Phys. Rev. A* **5**, 2338 (1972).
- ⁶²M. Eckhause *et al.*, *Nucl. Phys.* **81**, 575 (1966).
- ⁶³V. S. Evseev *et al.*, *Yad. Fiz.* **8**, 741 (1968) [*Sov. J. Nucl. Phys.* **8**, 431 (1969)].
- ⁶⁴D. E. Casperson *et al.*, *Phys. Lett.* **59B**, 397 (1975).
- ⁶⁵D. E. Casperson *et al.*, *Phys. Rev. Lett.* **38**, 956 (1977).
- ⁶⁶D. Favart *et al.*, *Phys. Rev. A* **8**, 1195 (1973).
- ⁶⁷K. P. Arnold *et al.*, report, Schweizerisches Institut für Nuklearforschung (SIN) Jahresbericht, 1978 (unpublished).
- ⁶⁸P. A. Souder *et al.*, LAMPF Proposal No. 268 (unpublished).
- ⁶⁹K. P. Arnold *et al.*, Eighth International Conference on High Energy Physics and Nuclear Structure, Vancouver, 1979 (unpublished); C. K. Gardner *et al.*, *Bull. Am. Phys. Soc.* **25**, 19 (1980).
- ⁷⁰T. D. Lee and C. S. Wu, *Annu. Rev. Nucl. Sci.* **15**, 381 (1965).
- ⁷¹M. A. Beg and G. Feinberg, *Phys. Rev. Lett.* **33**, 606 (1974); **35**, 130 (1975).
- ⁷²S. Weinberg, *Phys. Rev. Lett.* **19**, 1264 (1967); A. Salam, in *Elementary Particle Theory: Relativistic Groups and Analyticity (Noble Symposium No. 8)*, edited by N. Svartholm (Almqvist and Wiksell, Stockholm, 1968), p. 367.
- ⁷³J. Pati and A. Salam, *Phys. Rev. D* **10**, 274 (1974); R. N. Mohapatra and J. C. Pati, *Phys. Rev. D* **11**, 566 (1975); **11**, 2558 (1975).
- ⁷⁴T. Kinoshita, *Proceedings of the Nineteenth International Conference on High Energy Physics, Tokyo, 1978*, edited by S. Homma, M. Kawaguchi, and H. Miyazawa (Phys. Soc. of Japan, Tokyo, 1979), p. 571.